Switching sides—Reengineered primary charge separation in the bacterial photosynthetic reaction center

Philip D. Laible[a], Deborah K. Hanson[a], James C. Buhrmaster[a], Gregory A. Tira[a], Kaitlyn M. Faries[b], Dewey Holten[b], and Christine Kirmaier[b,1]

[a]Biosciences Division, Argonne National Laboratory, Lemont, IL 60439; and [b]Department of Chemistry, Washington University in St. Louis, St. Louis, MO 63130

Edited by Donald R. Ort, University of Illinois at Urbana–Champaign, Urbana, IL, and approved December 4, 2019 (received for review September 16, 2019)

We report 90% yield of electron transfer (ET) from the singlet excited state P* of the primary electron-donor P (a bacteriochlorophyll dimer) to the B-side bacteriopheophytin (H_B) in the bacterial photosynthetic reaction center (RC). Starting from a platform *Rhodobacter sphaeroides* RC bearing several amino acid changes, an Arg in place of the native Leu at L185—positioned over one face of H_B and only ∼4 Å from the 4 central nitrogens of the H_B macrocycle—is the key additional mutation providing 90% yield of $P^+H_B^-$. This all but matches the near-unity yield of A-side $P^+H_A^-$ charge separation in the native RC. The 90% yield of ET to H_B derives from (minimally) 3 P* populations with distinct means of P* decay. In an ∼40% population, P* decays in ∼4 ps via a 2-step process involving a short-lived $P^+B_B^-$ intermediate, analogous to initial charge separation on the A side of wild-type RCs. In an ∼50% population, P* → $P^+H_B^-$ conversion takes place in ∼20 ps by a superexchange mechanism mediated by B_B. An ∼10% population of P* decays in ∼150 ps largely by internal conversion. These results address the long-standing dichotomy of A- versus B-side initial charge separation in native RCs and have implications for the mechanism(s) and timescale of initial ET that are required to achieve a near-quantitative yield of unidirectional charge separation.

bacteriochlorophyll dimer | mutant reaction center | protein distributions | protein dynamics | ultrafast transient absorption spectroscopy

Conversion of light energy to chemical potential takes place in membrane-spanning reaction center (RC) proteins of photosynthetic bacteria, algae, and plants. Two transmembrane subunits harbor 2 quasisymmetric A and B chains, or branches of (bacterio)chlorophyll, (bacterio)pheophytin, and quinone. Fig. 1 shows the arrangement of the L, M, and H polypeptides and cofactors in RCs from *Rhodobacter sphaeroides* (1). P is a bacteriochlorophyll (BChl) dimer; B_A and B_B are monomeric BChls; H_A and H_B are bacteriopheophytins (BPhs); Q_A and Q_B are ubiquinones; and Fe is a nonheme iron. In bacterial RCs and photosystem II of plants and algae, only one branch of cofactors is used for photon-driven charge separation; in the bacterial RC, the A branch is active, and the B pathway is unused. The standard model for the free energies of the A- and B-side charge-separated (CS) states relative to P* in wild-type (WT) RCs from *R. sphaeroides* is shown in Fig. 2*A*. Initial charge separation in <10 ps and ∼100% yield occurs by a 2-step process: P* → $P^+B_A^-$ → $P^+H_A^-$. Several models for the time constants of these 2 electron-transfer (ET) steps have been presented (2–5). Both theory and experiments have shown that TyrM210 is key to positioning $P^+B_A^-$ slightly (∼70 meV) below P* in free energy, while symmetry-related PheL181 does not provide such stabilization of $P^+B_B^-$, which is thought to be ∼100 to 200 meV above P* (Figs. 1 and 2*A*) (6–13). State $P^+H_B^-$ also is higher in free energy than its A-side counterpart ($P^+H_A^-$) and may be only ∼70 meV below P* (14). Thus, normal electron flow in the WT RC is P* → $P^+B_A^-$ → $P^+H_A^-$ → $P^+Q_A^-$ → $P^+Q_B^-$; states $P^+B_B^-$ and $P^+H_B^-$ are not utilized.

Nearly quantitative redirection of the native initial charge-separation process to give $P^+H_B^-$ in *R. sphaeroides* RCs is reported here. This is achieved with an amino acid substitution near H_B—Arg replacing the native Leu at L185 (red in Fig. 1*B*)—in RCs also bearing a set of well-studied template, or background, substitutions of native amino acids shown in blue in Fig. 1*B*. The template mutations give a "starting point" advantage to B-side ET over A-side ET (15–17). TyrM210 near B_A is changed to Phe, and PheL181 near B_B is changed to Tyr. Consequently, compared to the WT RC, the free energy of $P^+B_A^-$ is higher, and the free energy of $P^+B_B^-$ is lower (Fig. 2*B* versus Fig. 2*A*). A third substitution, LeuM214 changed to His, results in replacement of H_A by a BChl denoted β_A. $P^+\beta_A^-$ (Fig. 2*B*) is higher in free energy than $P^+H_A^-$ in WT (Fig. 2*A*) and close to the position of $P^+B_A^-$ in WT (18, 19). We have previously shown that these 3 mutations in *R. sphaeroides* RCs result in ∼20% yield of P* → $P^+H_B^-$ and that additionally replacing ThrM133 with Glu increases the $P^+H_B^-$ yield to ∼60% (17). These 4 mutations are the core of 2 RC backgrounds used here, denoted bg1 and bg2. Both backgrounds also bear 2 mutations near Q_A (Fig. 1) that provide a double block on binding this cofactor (20, 21). The only difference between bg1 and bg2 is that in bg2, a Trp replaces the native Phe at L216 located between H_B and Q_B. Using both bg1 and bg2 templates, an Arg replaces the native Leu at

Significance

Photosynthetic organisms use pigment–protein complexes called reaction centers (RCs)—effectively nature's solar cells—to convert the energy of sunlight into charge-separated species that power life processes. Whether from plants, algae, or photosynthetic bacteria, RCs feature 2 quasi-mirror-image arrangements of protein and pigment cofactors. In RCs from purple photosynthetic bacteria, photon-induced electron transfer (ET) reduces the A-branch bacteriopheophytin (BPh) with near-unity quantum yield, while ET to the symmetry-related B-branch BPh is suppressed. Amino acid changes made here in the *Rhodobacter sphaeroides* RC nearly completely reverse this design. Specifically, we report RCs wherein ET to the B-branch BPh occurs with 90% yield. We draw insight regarding architectural and mechanistic foundations of the primary photon-driven charge-separation events of photosynthesis.

Author contributions: P.D.L., D.K.H., D.H., and C.K. designed research; D.K.H., J.C.B., G.A.T., K.M.F., and C.K. performed research; J.C.B., K.M.F, D.H., and C.K. analyzed data; and D.H. and C.K. wrote the paper.

The authors declare no competing interest.

This article is a PNAS Direct Submission.

[1]To whom correspondence may be addressed. Email: kirmaier@wustl.edu.

This article contains supporting information online at https://www.pnas.org/lookup/suppl/doi:10.1073/pnas.1916119117/-/DCSupplemental.

First published December 31, 2019.

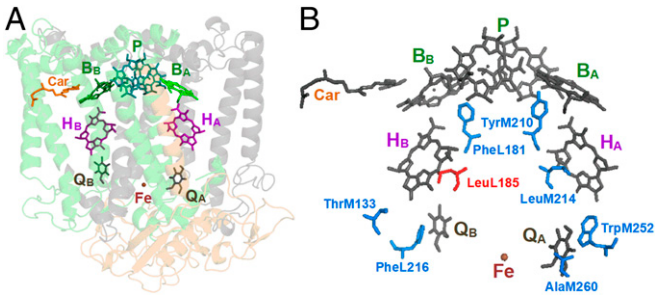

Fig. 1. (*A*) *R. sphaeroides* crystal structure (PDB ID code 1PCR) with polypeptides L (gray), M (green), and H (tan) and embedded cofactors: BChls (green), BPhs (purple), quinones (black), carotenoid (orange), and nonheme Fe (brown). Note that one helix of the L polypeptide lies near the B-side cofactors, and one helix of the M polypeptide lies near the A-side cofactors. (*B*) RC cofactors (gray) and the native amino acids (blue) that are substituted in 2 RC templates, bg1 and bg2, that differ only in having the native Phe at L216 (bg1) versus Trp at L216 (bg2). Using these 2 templates, the work here focuses on RCs bearing Arg in place of the native Leu at L185 (red).

L185, resulting in the Arg-bg1 and Arg-bg2 mutants studied here. These are part of 2 sets of mutants (to be reported elsewhere) where all amino acids have been substituted for LeuL185 in the bg1 and bg2 backgrounds. We show that ArgL185 makes $P^+H_B^-$ a better trap, supporting initial charge separation via a <10-ps 2-step mechanism in a portion of the P* population and via an ~20-ps superexchange mechanism in another portion—together providing near quantitative conversion of P* to $P^+H_B^-$.

Results

All results were obtained on RCs isolated and purified by using standard techniques and solubilized in 10 mM Tris (pH 7.8)/0.1% Deriphat 160-C buffer (*SI Appendix*). For all studies, Q_B was displaced from the RC by added terbutryn and Q_A by the mutational blocks noted above. The absence of both Q_A and Q_B enables high-repetition-rate ultrafast transient absorption (TA) experiments. Studies were performed on multiple biological replicate (BR) RCs for the Arg-bg1, Arg-bg2, bg1, and bg2 mutants. A BR is an RC obtained from an independently grown culture of cells originating from an archival frozen stock that came from a single colony carrying a plasmid of known sequence. Additionally, for some BRs of Arg-bg1, Arg-bg2, bg1, and bg2 RCs, repeat TA measurements were performed, where the same aliquot of RCs was reinterrogated following a freeze/storage/thaw cycle.

The yield of ET to H_B in Arg-bg1, Arg-bg2, and template bg1 and bg2 RCs was determined via TA spectroscopy and was based on comparison to the ~100% yield of ET from P* to H_A in the W(M252)V mutant (denoted WT^V), RCs which lack Q_A but otherwise are WT. In Fig. 3*A*, the $P^+H_A^-$ spectrum of WT^V RCs (black) shows the maximal bleaching of the Q_x absorption manifold of H_A, with $Q_x(0,0)$ and (1,0) vibronic bands at ~542 and ~507 nm, respectively. The H_A anion has a broad absorption band with a peak at ~665 nm. The orange, red, and blue spectra show comparable results for formation of $P^+H_B^-$ from 3 BRs of Arg-bg2 RCs. To make the comparisons shown in Fig. 3*A*, the ~0.3-ps P* spectrum of each Arg-bg2 BR was first normalized to the P bleaching at ~600 nm in the ~0.3-ps P* spectrum of WT^V. The normalization factor was then applied to the TA spectrum of the Arg-bg2 BR acquired at a (longer) time, where the amount of $P^+H_B^-$ was maximal. For each Arg mutant, the yield of $P^+H_B^-$ relative to the ~100% yield of $P^+H_A^-$ in WT^V was then determined by comparing the integrated magnitude of maximal bleaching of the H_B $Q_x(0,0)$ and (1,0) vibronic manifold to that for WT^V RCs (Fig. 3 *A*, *Inset* and *SI Appendix*, Fig. S1). The same $P^+H_B^-$ yields were obtained by comparing the peak amplitude of the H_B anion band (664 nm) of the mutants versus the H_A anion band (665 nm) of WT^V (Fig. 3*A*).

The largest Q_x integration value from 4 BRs of WT^V RCs was taken to reflect 100% yield of ET from P* to H_A. The other 3 BRs of WT^V gave values of 97%, 97%, and 93% (*SI Appendix*, Table S1). This narrow range indicates high precision of the TA experiments and Q_x bleaching integration method and/or only small natural variations of WT RC samples. Note that charge separation in WT *R. sphaeroides* RCs has a near-unity absolute quantum yield (22, 23). A 3- to 4-ps time constant for P* ET to B_A (2–4) in the native RC competing against 100- to 200-ps P* ET to H_B (15, 19, 24, 25) and 100- to 200-ps P* internal conversion (16) determines that P* in the WT RC decays ~2% by ET to H_B, ~2% to the ground state, and ~96% by ET to H_A (via B_A). As noted above, we took a value of 100% for A-side ET in WT in order to simplify comparison with the mutants.

Larger variability of the $P^+H_B^-$ yield was found for 3 initial BRs of Arg-bg2 RCs (75%, 87%, and 60%), ultimately prompting measurements on 15 BRs of RCs from Arg-bg2 and 6 BRs of Arg-bg1 (*SI Appendix*, Table S1). Additionally, for 9 BRs of Arg-bg2 and 3 BRs of Arg-bg1, repeat TA measurements were performed on the same aliquot of RCs after a freeze/storage/thaw cycle (*SI Appendix*, Table S1). The reproducibility of the yield of $P^+H_B^-$ determined from the 12 pairs of repeat TA experiments on BRs of Arg-bg1 and Arg-bg2 is ±3%. The sum total of results on the BRs (and repeat measurements) reveals that the highest (average ~90%) $P^+H_B^-$ yields are obtained for Arg-bg2 and Arg-bg1 RCs from midstationary phase cultures, and the lowest (60 to 70%) yields are obtained from late stationary phase cultures (*SI Appendix*, Table S1), which have higher culture density (Fig. 3*B*) and pH (Fig. 3*C*). Changes in RC spectral and kinetic properties with conditions (e.g., detergent and temperature) are well known (26–29). However, to our knowledge, dependence of RC photochemistry on culture density has not been reported. The underlying origin of these observations is not known at this time and is beyond the scope of this work.

The native Leu at L185 is positioned near one face of H_B (Fig. 3*C*) and is C_2-symmetry related to LeuM214 (Fig. 1*B*). One model of an Arg at L185 (in PyMOL) in the *R. sphaeroides* Protein Data Bank (PDB) ID code 1PCR structure (1) centers

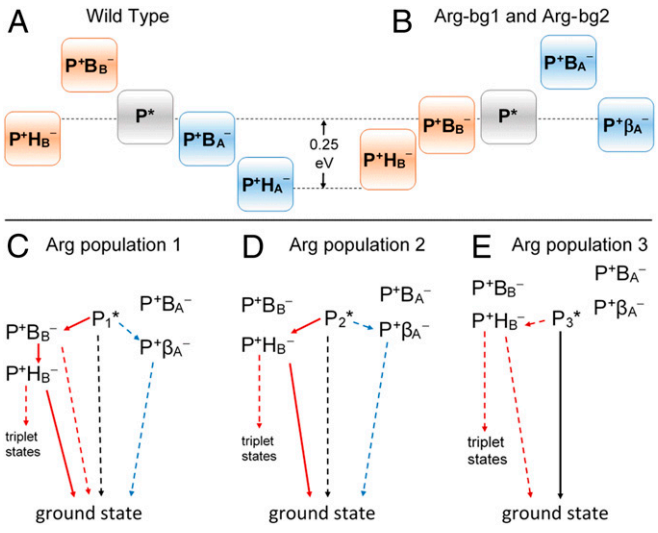

Fig. 2. (*A* and *B*) General model for the relative free energies of P* and CS states in WT RCs (*A*) and in Arg-bg1 and Arg-bg2 mutant RCs (*B*). P* is ~1.4 eV above the ground state. (*C*–*E*) Model state diagram for the major decay processes of 3 P* populations in Arg-bg1 and Arg-bg2 RCs: P_1*, τ ~4 ps (*C*); P_2*, τ ~20 ps (*D*); and P_3*, τ ~150 ps (*E*). Solid arrows indicate dominant processes, and dashed arrows reflect competing processes that have much lower yields.

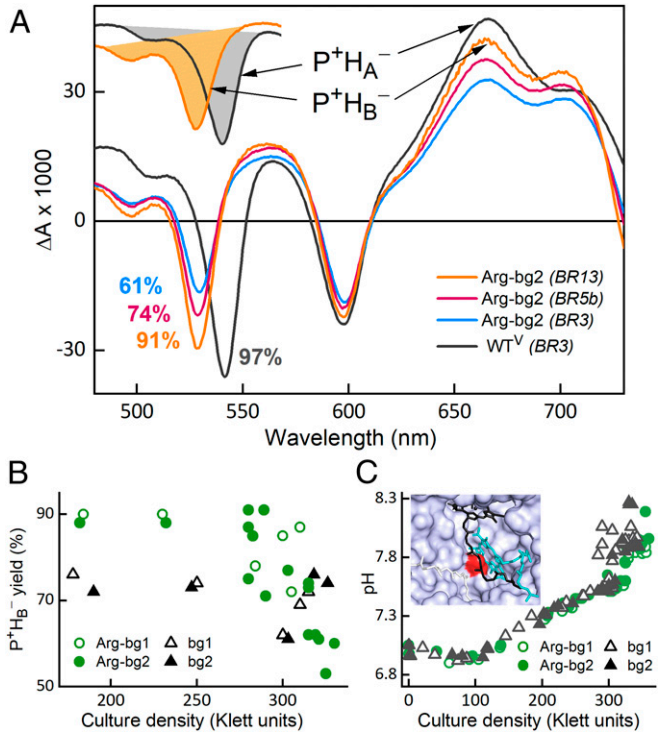

Fig. 3. (*A*) Ultrafast TA spectra for one BR of purified RCs of WT^V and 3 BRs of Arg-bg2 and yields of $P^+H_B^-$ (Arg variants) or $P^+H_A^-$ (WT^V). *A*, *Inset* shows the integrated Q_x bleaching manifold for Arg-bg2 BR13 (gold) and WT^V BR3 (gray). (*B*) $P^+H_B^-$ yield as a function of culture density of the cells from which RCs were isolated, for the BRs of Arg-bg1 and Arg-bg2 (green) and templates bg1 and bg2 (black). Three of the points for Arg-bg1 and 9 of the points for Arg-bg2 are the average values from pairs of repeat TA experiments, as listed in *SI Appendix*, Table S1. The average error in the yield of $P^+H_B^-$ determined from these 12 pairs of repeat measurements is ±3%. *SI Appendix*, Table S1 Graphic reproduces *B*, includes the individual error bars, and labels the points with their respective BR numbers given in *SI Appendix*, Table S1. (*C*) pH of *R. sphaeroides* cultures (7.05 at inoculation) as a function of culture density. *C*, *Inset* is a space-filling model of a portion of the *R. sphaeroides* RC protein (PDB ID code 1PCR) showing native LeuL185 (red) along with cofactors H_B (cyan), B_B (black), and Q_B (silver), including their phytyl chains (not shown in Fig. 1). An expanded version of *C*, *Inset* is given in *SI Appendix*, Fig. S64.

the Arg N_η atom ~4 Å from each of the 4 pyrrolic nitrogen atoms of H_B and ~6 Å from the ring-V keto group of H_B. Fig. 3*A* shows that the positions of the $Q_x(0,0)$ and $Q_x(1,0)$ bands of H_B in the ArgL185 mutants are blue shifted compared to those of H_A and do not vary as a function of $P^+H_B^-$ yield (or culture density).

The inherent (native) differences between the positions of the Q_x absorption bands of H_A and H_B have been described (17, 30–34). In brief, the A-side native GluL104 (thought to be neutral) forms a hydrogen bond to the ring-V keto group of H_A. Removing the hydrogen bond to H_A (substituting Leu for Glu at L104) blue shifts the Q_x bands of H_A by ~10 nm (30). On the B side, the residue that is related by C_2 symmetry to GluL104 is ThrM133, which is changed to Glu here in bg1, bg2, Arg-bg1, and Arg-bg2 RCs. Glu substituted at M133 is also thought to be neutral and make a hydrogen bond to H_B because this substitution is shown in prior work (17, 31–34) to red shift the Q_x bands of H_B by ~7 nm (*SI Appendix*, Table S2). We find here that the presence of ArgL185 results in a blue shift of the Q_x bands of H_B by ~7 nm in Arg-bg1 and Arg-bg2 RCs compared to bg1 and bg2 RCs (*SI Appendix*, Figs. S2 and S3 and Table S2). Similarly, the presence of ArgL185 in an analog that lacks GluM133 also gives a blue shift of the Q_x band of H_B (by ~5 nm) compared to the control RC with the native LeuL185 (*SI Appendix*, Table S2). At this time, we have no other independent information for bg1, bg2, or the Arg variants as to whether or when there is, or is not, any hydrogen bond to the ring-V keto group of H_B.

Discussion

Overview of the Analysis and Model. It is clear that an Arg at L185 influences the absorption properties of H_B, that this effect is invariant with $P^+H_B^-$ yield (Fig. 3*A*), and that the high ~90% yield of $P^+H_B^-$ is found for RCs isolated from cells harvested at lower culture density (Fig. 3*B*). Global analysis was performed on the ultrafast TA datasets (*SI Appendix*, Figs. S4–S11) of all 36 BRs of RCs from WT^V, TrpL216-WT^V, bg1, bg2, Arg-bg1, and Arg-bg2. The global analysis explored 5 to 9 exponentials (depending on sample) to obtain decay-associated difference spectra (DADS) (*SI Appendix*, Figs. S12–S57). The results were input into target analysis to obtain species-associated difference spectra (SADS) (*SI Appendix*, Figs. S58 and S59).

Even for WT RCs, it is well known that P* decay is not fit well by a single exponential. For Arg-bg1, Arg-bg2, bg1, and bg2 RCs, P* decay requires (minimally) 3 kinetic components with average lifetimes of P_1* ~4 ps, P_2* ~20 ps, and P_3* ~150 ps (*SI Appendix*, Fig. S60). Representing P* decay by 3 exponentials is the simplest distillation of what is likely to be a distribution of populations. Fig. 2 *C–E* gives a model for 3 populations having different free-energy orderings of the initial CS states with respect to an associated P* (P_1*, P_2*, and P_3*). Further, each state in the populations is viewed as having an intrinsic range of free energies, as depicted by the vertical size of the boxes in Fig. 2 *A* and *B* (but not shown in Fig. 2 *C–E*). Distributions can derive from both static and dynamic properties of the protein and cofactors and both have been invoked to explain multiexponential P* decay profiles in WT and mutant RCs (4, 7, 8, 33, 35–46).

Fig. 4*A* shows a correlation between a higher yield of $P^+H_B^-$ and a shorter amplitude-weighted average lifetime of P_1*, P_2*, and P_3*. Insight into this correlation is provided by Fig. 4*B* and *SI Appendix*, Table S3. As the $P^+H_B^-$ yield decreased from ~90 to ~60%, the proportion of P_3* (~150-ps lifetime) increased from ~10 to ~25%. An ~5% decrease in the abundance of P_1* (~4-ps lifetime) and an ~10% decrease of the abundance of P_2* (~20-ps lifetime) accounted for an ~15% increase in the amount of P_3*. The results are the same for the Arg-bg1 and Arg-bg2 variants.

We hypothesize that the presence of ArgL185 results in net stabilization of $P^+H_B^-$ (Fig. 2). Arg is considered normally to be protonated (pK_a = 12.7) (47). For example, in the RC, conserved and symmetry-related ArgL135 and ArgM164 residues have their N_η atom ~7.0 Å from the ring-V keto group (and ~13 Å from the

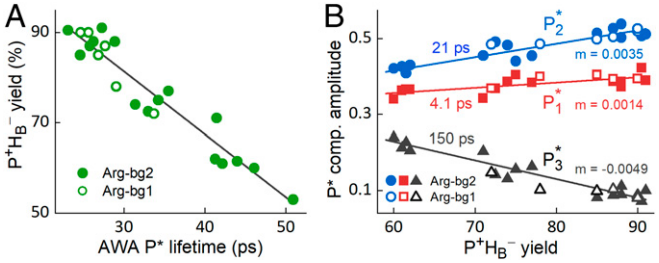

Fig. 4. P* decay properties in RCs from the 15 BRs of Arg-bg2 (filled symbols) and 6 BRs of Arg-bg1 (open symbols). *A* shows the yield of $P^+H_B^-$ versus the amplitude-weighted average (AWA) P* lifetime. *B* gives the fractional contribution of the 3 P* decay components (comp.) (Fig. 2 *C–E*) versus the yield of $P^+H_B^-$. *A* plots column 5 versus column 6 of *SI Appendix*, Table S3. *B* plots column 6 versus columns 2 (red, P_1*), 3 (blue, P_2*), and 4 (black, P_3*) of *SI Appendix*, Table S3. The reproducibility of the yield of $P^+H_B^-$ determined from the 12 pairs of *repeat* TA experiments on BRs of Arg-bg1 and Arg-bg2 is ±3% (*SI Appendix*, Table S1).

central Mg) of P_B and P_A, respectively. Both of these Arg residues are thought to be protonated, because replacing either Arg with Leu lowers the P/P^+ potential by 15 mV, and replacing either by Glu lowers it by 35 mV (48). The average P oxidation potential from a sampling of Arg-bg1 and Arg-bg2 RCs is ∼25 mV higher than for bg1 and bg2 RCs (*SI Appendix*, Table S4). The very close proximity of ArgL185 and H_B was noted above. If ArgL185 is protonated, the positive charge could make H_B significantly easier to reduce and (by inference, more than) offset the apparent increase in P oxidation potential. However, we have no direct knowledge, and draw no conclusion, as to whether ArgL185 is protonated in Arg-bg1 and Arg-bg2 RCs, or whether the protonation state of ArgL185 might vary among BRs of Arg-bg1 and Arg-bg2 RCs. Potential differences in water access to H_B or other structural or electrostatic effects associated with residues other than ArgL185 also could affect the free energy of $P^+H_B^-$. Regardless, Fig. 3*B* and our modeling analysis (Figs. 2 and 4) imply that stabilization of $P^+H_B^-$ by some means occurs to a greater degree or in a greater percentage of the RCs in samples with the higher $P^+H_B^-$ yields.

Global and Target Analysis. Using 2 representative BRs of Arg-bg2 and one BR of bg2, here we describe the distinctive DADS associated with P_1^*, P_2^*, and P_3^* that underlie the model in Fig. 2 *C*–*E*. The ∼4-ps DADS (Fig. 5 *A* and *E*) show characteristics consistent with 2-step $P_1^* \rightarrow P^+B_B^- \rightarrow P^+H_B^-$ ET. These included features (with appropriate signs) for P^+ (1,250 nm), a BChl anion (1,030 nm), both BChl and BPh anions (600 to 700 nm), BChl bleaching (600 nm), and BPh bleaching (529 nm for Arg-bg2 or 536 nm for bg2). In contrast, the ∼20-ps DADS (Fig. 5 *B* and *F*) are dominated by characteristics for $P_2^* \rightarrow P^+H_B^-$ conversion by superexchange ET. These include features for formation of H_B bleaching and H_B^- and P^+ absorption, along with substantial diminution of features for the BChl anion (see also below). The ∼150-ps DADS (Fig. 5 *C* and *G*) are comprised of features associated with P_3^* internal conversion to the ground state (decay of P bleaching at ∼600 and 830 to 870 nm). Such features are basically not present for P_1^* and are present for P_2^*, but to a much smaller extent. The ∼150-ps average P_3^* lifetime for the *R. sphaeroides* mutants studied here (*SI Appendix*, Table S5) is similar to the ∼180- to 200-ps P* internal conversion time measured for the *R. capsulatus* D_{LL} mutant RC where no ET occurs (16, 49) and for other *R. capsulatus* mutant RCs where P* → ground state competes effectively with various ratios of A- versus B-side ET (15, 19).

The different decay modes for P_1^*, P_2^*, and P_3^* indicated by the distinctive DADS underlie the 3-population model and differences between the relative free energies of the states seen in Fig. 2 *C*–*E*, respectively. A 3-population distillation is, again, a simplification of a distribution of P* populations. Results of target analysis indicate that the first step of $P_1^* \rightarrow P^+B_B^- \rightarrow P^+H_B^-$ ET has a time constant of ∼4 ps and that the time constant for the second step is similar or slightly longer. Not shown in Fig. 2 *C*–*E*, but included in the model for target analysis (*SI Appendix*, Fig. S58), is a small (∼10%) amount of $P^+H_B^-$ forming from $P^+B_B^-$ on the 20- to 30-ps timescale. For simplicity, this avenue of forming $P^+B_B^-$ was modeled as arising from P_2^* rather than introducing a fourth P* population. Potential contributions of both a "fast" and a "slow" 2-step process have been modeled for initial A-side ET in WT RCs (4). These points reinforce the complexity of the photochemistry and the DADS. Target analysis (*SI Appendix*, Fig. S58) returned nearly identical SADS (*SI Appendix*, Fig. S59) for P_1^*, P_2^*, and P_3^* that have the expected characteristics, notably, including absence of features for CS states, illustrating the consistency of the analysis.

The DADS associated with decay of the other products of P* decay—$P^+\beta_A^-$ (*SI Appendix*, Figs. S61 and S62) and $P^+H_B^-$ (Fig. 5 *D* and *H*)—show the expected features. The yield of $P^+\beta_A^-$ is 5% or less for Arg-bg2 RCs and 15 to 20% for bg2 RCs. $P^+\beta_A^-$ has an ∼1-ns lifetime and appears to decay in part by thermal repopulation of P* (*SI Appendix*, Fig. S58). Because Q_B is not present in the samples studied here, $P^+H_B^-$ decays by charge recombination partly to give the ground state (80 to 85% yield) and partly to give the triplet excited state (P^R) in 15 to 20% yield, which in turn decays by energy transfer to the carotenoid to give Car^T (*SI Appendix*, Figs. S61–S63). The $P^+H_B^-$ decay is fit adequately by a single exponential with a time constant of ∼12 ns for Arg-bg1 and Arg-bg2 RCs, but is dual-exponential with time constants of 3 and 12 ns for bg1 and bg2 RCs. The virtual absence of the ∼3-ns $P^+H_B^-$ decay component in Arg-bg1 and Arg-bg2 RCs can be explained by stabilization of $P^+H_B^-$ by ArgL185 (Fig. 2*B* versus Fig. 2*A*), reducing quantum/thermal mixing with P* and/or $P^+B_B^-$. We have discussed such mixing previously for various *R. capsulatus* mutants (34, 50, 51). Analogous mixing of A-side state $P^+H_A^-$ (52–55) or state $P^+\beta_A^-$ (18, 19, 56, 57) with $P^+B_A^-$ and/or P* has also been discussed.

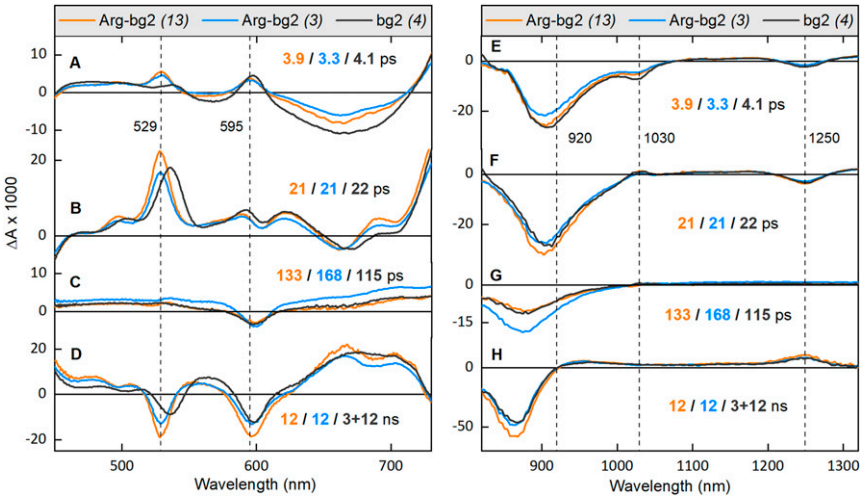

Fig. 5. (*A*–*C* and *E*–*G*) Comparison of visible (*A*–*C*) and near-infrared (*E*–*G*) DADS for the 3 P* decay components for Arg-bg2 BR13 (orange), Arg-bg2 BR3 (blue), and bg2 BR4 (black) RCs: ∼4-ps DADS (*A* and *E*), ∼20-ps DADS (*B* and *F*), and ∼150-ps DADS (*C* and *G*). (*D* and *H*) DADS associated with $P^+H_B^-$, which forms with a yield of 0.91 (Arg-bg2 BR13), 0.61 (Arg-bg2 BR3), and 0.73 (bg2 BR4); the DADS for bg2 is the sum of 3- and 12-ns subcomponent spectra.

Collectively, our results show that replacing Leu185 with Arg has more than one effect that supports B-side charge separation. *1*) ArgL185 complements the template mutations (notably, changing TyrM210 to Phe) in significantly slowing ET to the A side (*SI Appendix*, Table S5). This effect can be traced to the ∼25-mV higher P/P^+ potential when L185 was Arg versus the native Leu (*SI Appendix*, Table S4). This will elevate $P^+B_A^-$ and $P^+\beta_A^-$ in free energy by ∼25 meV. *2*) While the B-side CS states will be similarly elevated in free energy by the increased P oxidation potential, our results indicate (as mentioned above) that there is a larger local stabilizing effect of Arg on the free energy of $P^+H_B^-$. Specifically, the presence of ArgL185 makes H_B (and perhaps B_B) easier to reduce. This underlies the increased yield of $P^+H_B^-$ due to a larger contribution of 2-step ET and an increased superexchange rate constant as well. A pronounced local effect on H_B is reasonable in view of PyMOL models that replace LeuL185 with Arg in the *R. sphaeroides* crystal structure, which indicates that ArgL185 could be only ∼4 Å from each of the 4 central pyrrolic nitrogen atoms of H_B. *3*) Replacing Leu by Arg at L185 slows $P^+H_B^-$ charge recombination to ∼12 ns. This is the longest time constant for this process found to date and is comparable to the ∼15-ns A-side $P^+H_A^-$ charge recombination time (when Q_A is absent) (58, 59). Slower $P^+H_B^-$ charge recombination and the F(L216)W mutation in the bg2 template both should improve $P^+H_B^- \rightarrow P^+Q_B^-$ ET.

Unifying RC Distributions, Relaxations, and Complex Dynamics. The electronic structure of P and how it is perturbed by excitation may link many complexities of RC dynamics. The logic behind this follows. Protein motions afford a fluctuating environment for the RC cofactors, temporally modulating their electronic structures and redox properties. At a snapshot in time, these will differ among RCs in a sample. At the instant of excitation, the ensemble will be mapped onto a P* potential energy surface(s), and subsequent protein-cofactor motions can alter the distribution of populations. Protein motions may limit ET rates (40). They may also contribute to free-energy relaxations of $P^+H_A^-$ ranging from <1 to >10 ns when ET to Q_A is blocked (52, 53, 55, 60, 61). Complex kinetics were also found for $P^* \rightarrow P^+B_A^- \rightarrow P^+H_A^-$ and $P^+H_A^- \rightarrow P^+Q_A^-$ in WT RCs, implying multiple populations (4, 37). P* populations that exhibit different photochemistry, such as seen here, also have been described for various mutants (9, 33, 44, 62). These findings, the data here, and the model in Fig. 2 *C–E* can be unified by considering a trigger that abruptly alters the fluctuating ensemble of protein/cofactor interactions/energetics at the instant of excitation of P, over and above effects due simply to adding excitation energy.

A change in the physical/electronic structure of P upon excitation might be such a trigger. This will simultaneously affect the free-energy ranges (i.e., the vertical sizes of the boxes in Fig. 2 *A* and *B*) of all of the electronic states of the RC (Fig. 2 *C–E*) because they all involve P. The electronic structure of P can be viewed in analogy to the properties of strongly coupled tetrapyrrole dimers (63–68). The highest occupied molecular orbital (HOMO) of P is an antibonding MO at higher energy than the HOMOs of the constituent BChls (P_A and P_B) due to interactions between the 2 BChls. (This makes P easier to oxidize than a BChl monomer.) The dimer lowest unoccupied molecular orbital (LUMO) is a bonding combination of the LUMOs of P_A and P_B. Excitation of P to P* promotes an electron from the antibonding HOMO to the bonding LUMO and shifts electron density from the outward faces of P_A and P_B into the region between P_A and P_B. This increases the interaction between P_A and P_B, which reduces the P_A–P_B distance and raises the HOMO in energy. This increase in HOMO energy makes P* easier to oxidize over and above the general effect that an excited state of a molecule is easier to oxidize than its ground state. Because P* is easier to oxidize (than it would have been had the P_A–P_B distance not been reduced upon excitation), the free energies of all of the CS states will be lower than they were at the P_A–P_B distance in the ground state. Ensuing oxidation of P* to P^+ via ET removes the electron in the bonding LUMO, shifting the P_A–P_B distance to a value intermediate between those for P* and P, raising the P/P^+ potential and free energies of all of the CS states, again potentially affecting the vertical sizes of the boxes in Fig. 2 *A* and *B*. Any of these effects, starting at excitation of P to P*, could promote protein dynamics, some of which might contribute to dielectric relaxations in response to charge separation (55, 61).

Motions that alter the interactions and distance between the 2 macrocycles of P have been proposed to be important for the spectral and redox properties of P and for P* ET dynamics (45, 65, 69–72). Such motions also likely underlie the much shorter (100 to 200 ps) time constant for P* internal conversion compared to that (∼5 ns) for excited monomeric BChl* (73). A related view is that fluctuations of distance between the 2 macrocycles of P alter the admixture of the charge-resonance and exciton (or charge-transfer and locally excited) configurations of P*. Thus, the electronic structure of P and how it is perturbed by excitation may link many complexities of RC dynamics. This includes the nature of the distributions that are central to our analysis of how the very high, ∼90%, yield of B-side charge separation is attained.

Two-step $P^* \rightarrow P^+B_B^- \rightarrow P^+H_B^-$ ET mimics $P^* \rightarrow P^+B_A^- \rightarrow P^+H_A^-$ charge separation on the A side in the native RC. The ∼90% yield of $P^+H_B^-$ is achieved by comparable contributions of this 2-step process and slower (∼20 ps) $P^* \rightarrow P^+H_B^-$ superexchange. A residual ∼10% of P* decay occurs mainly by internal conversion to the ground state. These results have many interesting consequences that should provoke additional experiments and theoretical analysis. It is possible that RCs employing comparable contributions of the 2 mechanisms for A-side charge separation may have existed during evolution of the photosynthetic apparatus. If such RCs (analogous to those studied here) had been a stepping stone, our results show that further tuning of the relative free energies of the CS states to convert the ∼50% superexchange population into a "2-step" population would gain only the last 5 to 10% of the near-unity yield of A-side charge separation.

Materials and Methods

Complete descriptions of sample preparation, static and time-resolved optical spectroscopy, and analysis of TA datasets are given in *SI Appendix*.

Data Availability. All data needed to support the conclusions of this manuscript are included in the main text and *SI Appendix*. *R. sphaeroides* strains are available upon request.

ACKNOWLEDGMENTS. We thank Dr. David Bocian for helpful discussion and Abby Gibbons for measurements of pH and densities of cultures. This work was supported by the US Department of Energy, Office of Basic Energy Sciences Grant DE-CD0002036 (to C.K. and D.H.) and associated Field Work Proposal (P.D.L.). Argonne, a US Department of Energy Office of Science laboratory, is operated under Contract DE-AC02-06CH11357.

1. U. Ermler, G. Fritzsch, S. K. Buchanan, H. Michel, Structure of the photosynthetic reaction centre from *Rhodobacter sphaeroides* at 2.65 A resolution: Cofactors and protein-cofactor interactions. *Structure* **2**, 925–936 (1994).
2. W. Zinth, J. Wachtveitl, The first picoseconds in bacterial photosynthesis—Ultrafast electron transfer for the efficient conversion of light energy. *ChemPhysChem* **6**, 871–880 (2005).
3. Y. Kakitani, A. Hou, Y. Miyasako, Y. Koyama, H. Nagae, Rates of the initial two steps of electron transfer in reaction centers from *Rhodobacter sphaeroides* as determined by singular-value decomposition followed by global fitting. *Chem. Phys. Lett.* **492**, 142–149 (2010).
4. J. Zhu, I. H. M. van Stokkum, L. Paparelli, M. R. Jones, M. L. Groot, Early bacteriopheophytin reduction in charge separation in reaction centers of *Rhodobacter sphaeroides*. *Biophys. J.* **104**, 2493–2502 (2013).
5. A. G. Yakovlev, A. Y. Shkuropatov, V. A. Shuvalov, Nuclear wavepacket motion between P and P(+)B(A)(-) potential surfaces with subsequent electron transfer to H(A) in bacterial reaction centers. 1. Room temperature. *Biochemistry* **41**, 2667–2674 (2002).

6. R. G. Alden, W. W. Parson, Z. T. Chu, A. Warshel, Orientation of the OH dipole of tyrosine (M)210 and its effect on electrostatic energies in photosynthetic bacterial reaction centers. *J. Phys. Chem.* **100**, 16761–16770 (1996).
7. M. Bixon, J. Jortner, M. E. Michel-Beyerle, A kinetic analysis of the primary charge separation in bacterial photosynthesis. Energy gaps and static heterogeneity. *Chem. Phys.* **197**, 389–404 (1995).
8. G. Hartwich, H. Lossau, M. E. Michel-Beyerle, A. Ogrodnik, Nonexponential fluorescence decay in reaction centers of *Rhodobacter sphaeroides* reflecting dispersive charge separation up to 1 ns. *J. Phys. Chem. B* **102**, 3815–3820 (1998).
9. M. Saggu *et al*., Putative hydrogen bond to tyrosine M208 in photosynthetic reaction centers from *Rhodobacter capsulatus* significantly slows primary charge separation. *J. Phys. Chem. B* **118**, 6721–6732 (2014).
10. S. Schmidt *et al*., Energetics of the primary electron transfer reaction revealed by ultrafast spectroscopy on modified bacterial reaction centers. *Chem. Phys. Lett.* **223**, 116–120 (1994).
11. M. R. Gunner, A. Nicholls, B. Honig, Electrostatic potentials in *Rhodopseudomonas viridis* reaction centers: Implications for the driving force and directionality of electron transfer. *J. Phys. Chem.* **100**, 4277–4291 (1996).
12. A. Warshel, Z. T. Chu, W. W. Parson, On the energetics of the primary electron-transfer process in bacterial reaction centers. *J Photochem. Photobiol A.* **82**, 123–128 (1994).
13. E. Katilius *et al*., Manipulations of the B-side charge-separated states' energetics in the Rhodobacter sphaeroides reaction center. *J. Phys. Chem. B* **107**, 12029–12034 (2003).
14. E. Katilius, Z. Katiliene, S. Lin, A. K. W. Taguchi, N. W. Woodbury, B-side electron transfer in the HE(M182) reaction center mutant from *Rhodobacter sphaeroides*. *J. Phys. Chem. B* **106**, 12344–12350 (2002).
15. C. Kirmaier, C. He, D. Holten, Manipulating the direction of electron transfer in the bacterial reaction center by swapping Phe for Tyr near $BChl_{(M)}$ (L181) and Tyr for Phe near $BChl_{(L)}$ (M208). *Biochemistry* **40**, 12132–12139 (2001).
16. J. I. Chuang, S. G. Boxer, D. Holten, C. Kirmaier, High yield of M-side electron transfer in mutants of *Rhodobacter capsulatus* reaction centers lacking the L-side bacteriopheophytin. *Biochemistry* **45**, 3845–3851 (2006).
17. N. P. Dylla *et al*., Species differences in unlocking B-side electron transfer in bacterial reaction centers. *FEBS Lett.* **590**, 2515–2526 (2016).
18. C. Kirmaier, D. Gaul, R. DeBey, D. Holten, C. C. Schenck, Charge separation in a reaction center incorporating bacteriochlorophyll for photoactive bacteriopheophytin. *Science* **251**, 922–927 (1991).
19. B. A. Heller, D. Holten, C. Kirmaier, Control of electron transfer between the L- and M-sides of photosynthetic reaction centers. *Science* **269**, 940–945 (1995).
20. W. J. Coleman, E. J. Bylina, D. C. Youvan, "Reconstitution of photochemical activity in *Rhodobacter capsulatus* reaction centers containing mutation at tryptophan M-250 in the primary quinone binding site" in *Current Research in Photosynthesis*, M. Baltscheffsky, Ed. (Kluwer, Dordrecht, Netherlands, 1990), pp. 149–152.
21. M. C. Wakeham, D. Frolov, P. K. Fyfe, R. van Grondelle, M. R. Jones, Acquisition of photosynthetic capacity by a reaction centre that lacks the $Q(_A)$ ubiquinone; possible insights into the evolution of reaction centres? *Biochim. Biophys. Acta* **1607**, 53–63 (2003).
22. C. A. Wraight, R. K. Clayton, The absolute quantum efficiency of bacteriochlorophyll photooxidation in reaction centres of *Rhodopseudomonas spheroides*. *Biochim. Biophys. Acta* **333**, 246–260 (1974).
23. R. K. Clayton, T. Yamamoto, Photochemical quantum efficiency and absorption-spectra of reaction centers from *Rhodopseudomonas-sphaeroides* at low-temperature. *Photochem. Photobiol.* **24**, 67–70 (1976).
24. C. Kirmaier *et al*., Comparison of M-side electron transfer in *Rb. sphaeroides* and *Rb. capsulatus* reaction centers. *J. Phys. Chem. B* **106**, 1799–1808 (2002).
25. C. Kirmaier, P. D. Laible, D. K. Hanson, D. Holten, B-side electron transfer to form $P^+H_B^-$ in reaction centers from the F(L181)Y/Y(M208)F mutant of *Rhodobacter capsulatus*. *J. Phys. Chem. B* **108**, 11827–11832 (2004).
26. C. Kirmaier, D. Holten, W. W. Parson, Picosecond photodichroism studies of the transient states in *Rhodopseudomonas sphaeroides* reaction centers at 5K. Effects on electron transfer on the six bacteriochlorin pigments. *Biochem. Biophys. Acta* **810**, 49–61 (1985).
27. C. Kirmaier, D. Holten, W. W. Parson, Temperature and detection-wavelength dependence of the picosecond electron-transfer kinetics measured in *Rhodopseudomonas sphaeroides* reaction centers. Resolution of new spectral and kinetic components in the primary charge-separation process. *Biochem. Biophys. Acta* **810**, 33–48 (1985).
28. S. Lin, W. Xiao, J. E. Eastman, A. K. W. Taguchi, N. W. Woodbury, Low-temperature femtosecond-resolution transient absorption spectroscopy of large-scale symmetry mutants of bacterial reaction centers. *Biochemistry* **35**, 3187–3196 (1996).
29. J. E. Eastman, A. K. W. Taguchi, S. Lin, J. A. Jackson, N. W. Woodbury, Characterization of a *Rhodobacter capsulatus* reaction center mutant that enhances the distinction between spectral forms of the initial electron donor. *Biochemistry* **39**, 14787–14798 (2000).
30. E. J. Bylina, C. Kirmaier, L. M. McDowell, D. Holten, D. C. Youvan, Influence of an amino acid residue on the optical properties and electron transfer dynamics of a photosynthetic reaction center complex. *Nature* **336**, 182–184 (1988).
31. F. Müh, J. C. Williams, J. P. Allen, W. Lubitz, A conformational change of the photoactive bacteriopheophytin in reaction centers from *Rhodobacter sphaeroides*. *Biochemistry* **37**, 13066–13074 (1998).
32. C. Kirmaier, A. Cua, C. He, D. Holten, D. F. Bocian, Probing M-branch electron transfer and cofactor environment in the bacterial photosynthetic reaction center by the addition of a hydrogen bond to the M-side bacteriopheophytin. *J. Phys. Chem. B* **106**, 495–503 (2002).
33. B. Carter, S. G. Boxer, D. Holten, C. Kirmaier, Photochemistry of a bacterial photosynthetic reaction center missing the initial bacteriochlorophyll electron acceptor. *J. Phys. Chem. B* **116**, 9971–9982 (2012).
34. K. M. Faries *et al*., Optimizing multi-step B-side charge separation in photosynthetic reaction centers from *Rhodobacter capsulatus*. *Biochim. Biophys. Acta* **1857**, 150–159 (2016).
35. L. M. P. Beekman *et al*., Primary electron transfer in membrane-bound reaction centers with mutations at the M210 position. *J. Phys. Chem.* **100**, 7256–7268 (1996).
36. M. Du *et al*., Femtosecond spontaneous-emission studies of reaction centers from photosynthetic bacteria. *Proc. Natl. Acad. Sci. U.S.A.* **89**, 8517–8521 (1992).
37. C. Kirmaier, D. Holten, Evidence that a distribution of bacterial reaction centers underlies the temperature and detection-wavelength dependence of the rates of the primary electron-transfer reactions. *Proc. Natl. Acad. Sci. U.S.A.* **87**, 3552–3556 (1990).
38. P. D. Laible, S. R. Greenfield, M. R. Wasielewski, D. K. Hansen, R. M. Pearlstein, Antenna excited state decay kinetics establish primary electron transfer in reaction centers as heterogeneous. *Biochemistry* **36**, 8677–8685 (1997).
39. J. M. Peloquin, S. Lin, A. K. W. Taguchi, N. W. Woodbury, Excitation wavelength dependence of bacterial reaction center photochemistry. 2. Low-temperature measurements and spectroscopy of charge separation. *J. Phys. Chem.* **100**, 1428–14235 (1996).
40. H. Wang *et al*., Protein dynamics control the kinetics of initial electron transfer in photosynthesis. *Science* **316**, 747–750 (2007).
41. A. R. Holzwarth, M. G. Müller, Energetics and kinetics of radical pairs in reaction centers from *Rhodobacter sphaeroides*. A femtosecond transient absorption study. *Biochemistry* **35**, 11820–11831 (1996).
42. P. Hamm *et al*., Subpicosecond emission studies of bacterial reaction centers. *Biochim. Biophys. Acta* **1142**, 99–105 (1993).
43. M. G. Muller, K. Griebenow, A. R. Holzarth, Primary processes in isolated bacterial reaction centers from *Rhodobacter sphaeroides* studied by picosecond fluorescence kinetics. *Chem. Phys. Lett.* **199**, 465–469 (1992).
44. C. Kirmaier, P. D. Laible, E. Hinden, D. K. Hanson, D. Holten, Detergent effects on primary charge separation in wild-type and mutant *Rhodobacter capsulatus* reaction centers. *Chem. Phys.* **294**, 305–318 (2003).
45. M. H. Vos *et al*., Direct observation of vibrational coherence in bacterial reaction centers using femtosecond absorption spectroscopy. *Proc. Natl. Acad. Sci. U.S.A.* **88**, 8885–8889 (1991).
46. V. Nagarajan, W. W. Parson, D. Davis, C. C. Schenck, Kinetics and free energy gaps of electron-transfer reactions in *Rhodobacter sphaeroides* reaction centers. *Biochemistry* **32**, 12324–12336 (1993).
47. M. J. Harms, J. L. Schlessman, G. R. Sue, B. García-Moreno, Arginine residues at internal positions in a protein are always charged. *Proc. Natl. Acad. Sci. U.S.A.* **108**, 18954–18959 (2011).
48. E. T. Johnson *et al*., Electronic and vibronic coupling of the special pair of bacteriochlorophylls in photosynthetic reaction centers from wild-type and mutant strains of *Rhodobacter sphaeroides*. *J. Phys. Chem. B* **106**, 11859–11869 (2002).
49. J. Breton, J. L. Martin, J. C. Lambry, S. J. Robles, D. C. Youvan, "Ground state and femtosecond transient absorption spectroscopy of a mutant of *Rhodobacter capsulatus* which lacks the initial electron acceptor bacteriopheophyrin" in *Structure and Function of Bacterial Photosynthetic Reaction Centers*, M. E. Michel-Beyerle, Ed. (Springer-Verlag, New York, 1990), pp. 293–302.
50. L. Kressel *et al*., High yield of secondary B-side electron transfer in mutant *Rhodobacter capsulatus* reaction centers. *Biochim. Biophys. Acta* **1837**, 1892–1903 (2014).
51. K. M. Faries *et al*., Manipulating the energetics and rates of electron transfer in *Rhodobacter capsulatus* reaction centers with asymmetric pigment content. *J. Phys. Chem. B* **121**, 6989–7004 (2017).
52. N. W. Woodbury *et al*., Relationship between thermodynamics and mechanism during photoinduced charge separation in reaction centers from *Rhodobacter sphaeroides*. *Biochemistry* **33**, 8101–8112 (1994).
53. K. Gibasiewicz *et al*., Analysis of the temperature-dependence of $P(^{+})H_A(^{-})$ charge recombination in the *Rhodobacter sphaeroides* reaction center suggests nanosecond temperature-independent protein relaxation. *Phys. Chem. Chem. Phys.* **15**, 16321–16333 (2013).
54. J. Pan *et al*., The protein environment of the bacteriopheophytin anion modulates charge separation and charge recombination in bacterial reaction centers. *J. Phys. Chem. B* **117**, 7179–7189 (2013).
55. K. Dubas, M. Baranowski, A. Podhorodecki, M. R. Jones, K. Gibasiewicz, Unified model of nanosecond charge recombination in closed reaction centers from *Rhodobacter sphaeroides*: Role of protein polarization dynamics. *J. Phys. Chem. B* **120**, 4890–4896 (2016).
56. L. Laporte, L. M. McDowell, C. Kirmaier, C. C. Schenck, D. Holten, Insights into the factors controlling the rates of the deactivation processes that compete with charge separation in photosynthetic reaction centers. *Chem. Phys.* **176**, 615–629 (1993).
57. J. Pan, R. Saer, S. Lin, J. T. Beatty, N. W. Woodbury, Electron transfer in bacterial reaction centers with the photoactive bacteriopheophytin replaced by a bacteriochlorophyll through coordinating ligand substitution. *Biochemistry* **55**, 4909–4918 (2016).
58. C.-K. Tang, J. C. Williams, A. K. W. Taguchi, J. P. Allen, N. W. Woodbury, P+HA- charge recombination reaction rate constant in *Rhodobacter sphaeroides* reaction centers is independent of the P/P+ midpoint potential. *Biochemistry* **38**, 8794–8799 (1999).
59. K. Gibasiewicz *et al*., Mechanism of recombination of the $P^+H(_A^-)$ radical pair in mutant *Rhodobacter sphaeroides* reaction centers with modified free energy gaps between $P^+B(_A^-)$ and $P^+H(_A^-)$. *J. Phys. Chem. B* **115**, 13037–13050 (2011).
60. A. Ogrodnik, W. Keupp, M. Volk, G. Aumeier, M. E. Michel-Beyerle, Inhomogeneity of radical pair energies in photosynthetic reaction centers revealed by differences in recombination dynamics of P^+H^- when detected in delayed emission and in absorption. *J. Phys. Chem.* **98**, 3432–3439 (1994).

61. Z. Guo, N. W. Woodbury, J. Pan, S. Lin, Protein dielectric environment modulates the electron-transfer pathway in photosynthetic reaction centers. *Biophys. J.* **103**, 1979–1988 (2012).
62. K. M. Faries *et al*., Consequences of saturation mutagenesis of the protein ligand to the B-side monomeric bacteriochlorophyll in reaction centers from *Rhodobacter capsulatus*. *Photosynth. Res.* **141**, 273–290 (2019).
63. R. J. Donohoe, J. K. Duchowski, D. F. Bocian, Hole delocalization in oxidized cerium(IV) porphyrin sandwich complexes. *J. Am. Chem. Soc.* **110**, 6119–6124 (1988).
64. O. Bilsel *et al*., Electronic states and optical properties of porphyrins in van der Waals contact: Thorium(IV) sandwich complexes. *J. Am. Chem. Soc.* **114**, 6528–6538 (1992).
65. A. Warshel, Role of the chlorophyll dimer in bacterial photosynthesis. *Proc. Natl. Acad. Sci. U.S.A.* **77**, 3105–3109 (1980).
66. M. A. Thompson, M. Zerner, J. Fajer, A theoretical examination of the electronic structure and excited states of the bacteriochlorophyll b dimer from *Rhodopseudomonas viridis*. *J. Phys. Chem.* **95**, 5693–5700 (1991).
67. P. O. J. Scherer, S. F. Fischer, Quantum treatment of the optical spectra and the initial electron transfer process within the reaction center of *Rhodopseudomonas viridis*. *Chem. Phys.* **131**, 115–127 (1989).
68. H. S. Kang *et al*., Effects of strong electronic coupling in chlorin and bacteriochlorin dyads. *J. Phys. Chem. A* **120**, 379–395 (2016).
69. V. Tiwari, W. K. Peters, D. M. Jonas, Electronic resonance with anticorrelated pigment vibrations drives photosynthetic energy transfer outside the adiabatic framework. *Proc. Natl. Acad. Sci. U.S.A.* **110**, 1203–1208 (2013).
70. T. R. Middendorf, L. T. Mazzola, D. F. Gaul, C. C. Schenck, S. G. Boxer, Photochemical hole-burning spectroscopy of a photosynthetic reaction center mutant with altered charge separation kinetics: Properties and decay of the initially excited-state. *J. Phys. Chem.* **95**, 10142–10151 (1991).
71. K. Czarnecki *et al*., Characterization of the strongly coupled, low-frequency vibrational modes of the special pair of photosynthetic reaction centers via isotopic labeling of the cofactors. *J. Am. Chem. Soc.* **119**, 415–426 (1997).
72. S. G. Johnson *et al*., Primary donor state mode structure and energy-transfer in bacterial reaction centers. *J. Phys. Chem.* **94**, 5849–5855 (1990).
73. L. M. McDowell, D. Gaul, C. Kirmaier, D. Holten, C. C. Schenck, Investigation into the source of electron transfer asymmetry in bacterial reaction centers. *Biochemistry* **30**, 8315–8322 (1991).